Supplementary Information

Table S1 - Summary of sintering conditions and calculated densities for pellets of $Li_{2+x}Ni_{2-2x}Cr_xV_2O_8$ (x = 0, 0.25, 0.5, 0.75 and 1) used in impedance spectroscopy.

Composition, x	Sintering conditions	Density / g cm^{-3}	Theoretical density / g cm^{-3}	Density / %
0.00	650 °C, 12 h	3.270	4.319	76
0.25	650 °C, 12 h	3.140	4.153	76
0.50	650 °C, 12 h	3.040	3.984	76
0.75	650 °C, 12 h	3.217	3.816	84
1.00	550 °C, 12 h	2.160	3.644	59

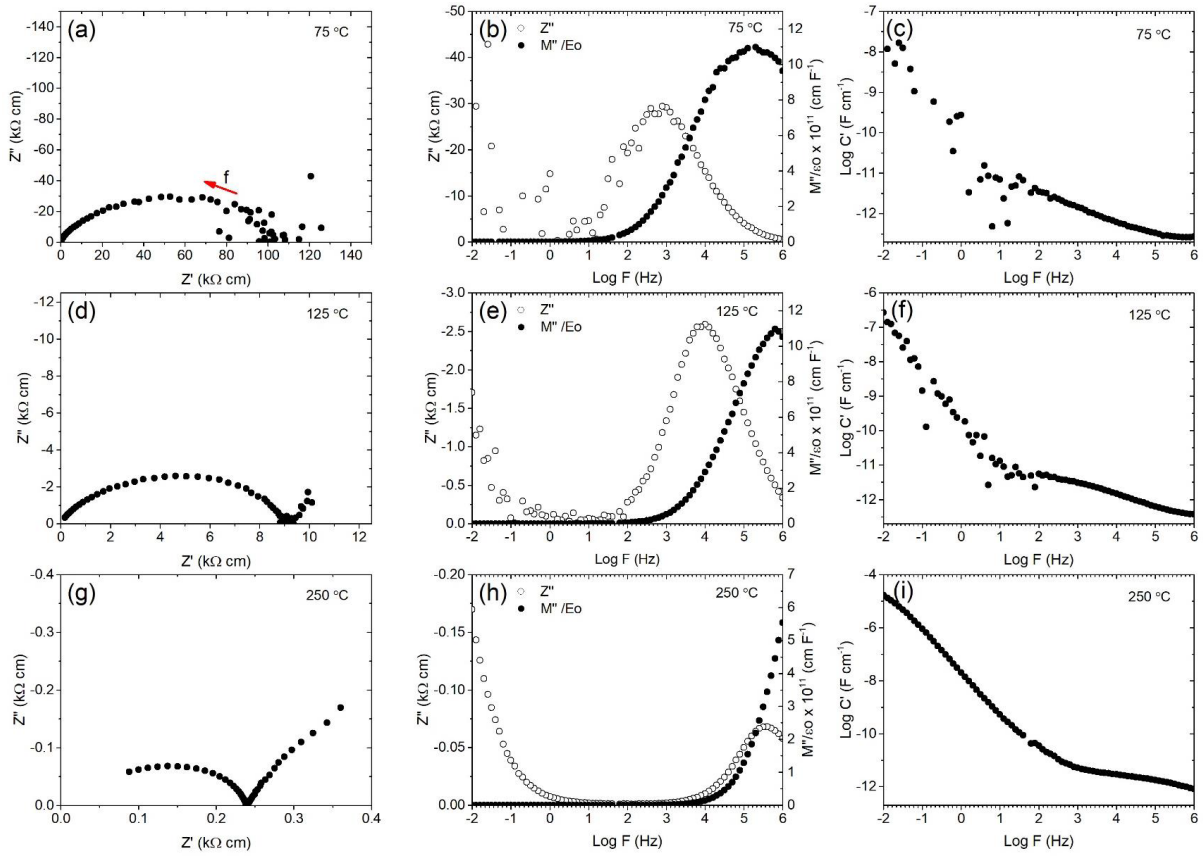

Figure S1 - Impedance complex plane plots (a, d, g) and spectroscopic plots of C'(c, f, i), M" and -Z" (b, e, h) for $Li_2Ni_2V_2O_8$ at 75 °C, 125 °C and 250 °C.

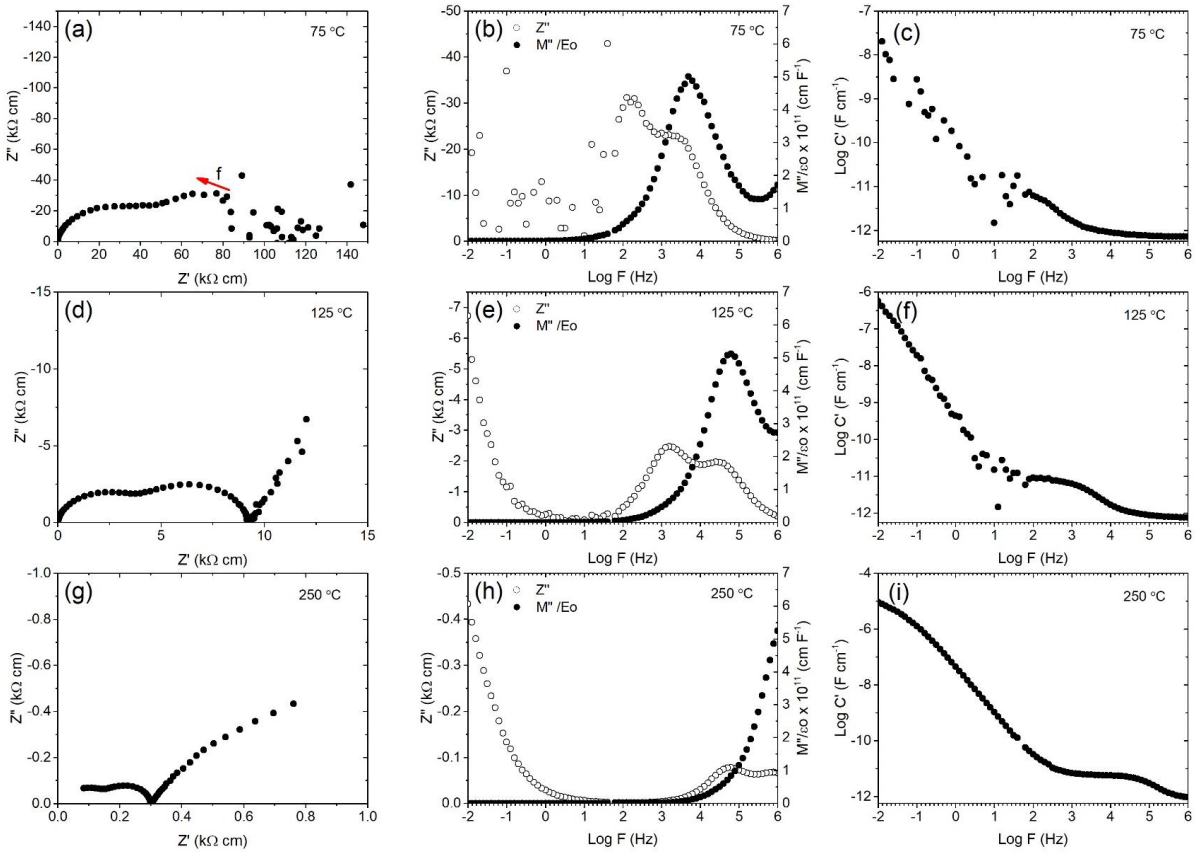

Figure S2 - Impedance complex plane plots (a, d, g) and spectroscopic plots of C'(c, f, i), M" and -Z" (b, e, h) for $Li_{2.25}Ni_{1.5}Cr_{0.25}V_2O_8$ at 75 °C, 125 °C and 250 °C.

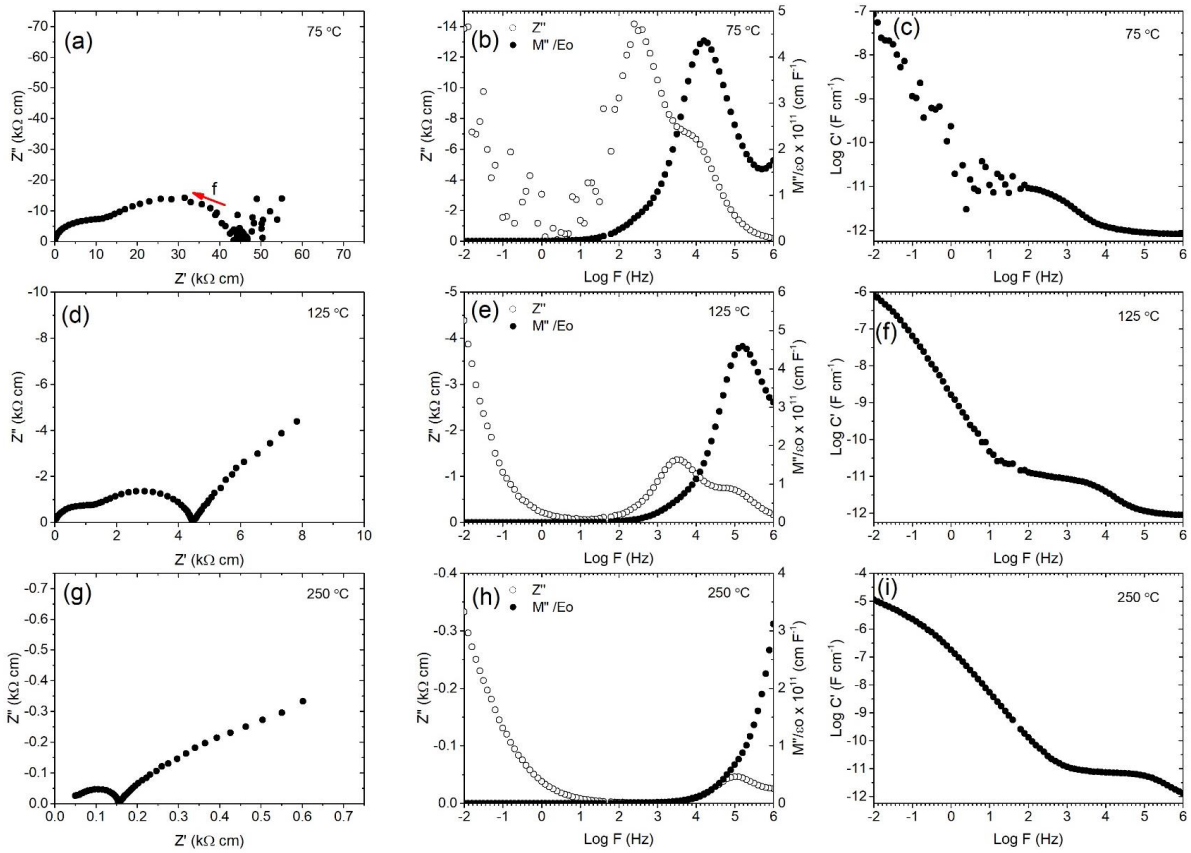

Figure S3 - Impedance complex plane plots (a, d, g) and spectroscopic plots of C'(c, f, i), M" and -Z" (b, e, h) for $Li_{2.5}Ni_1Cr_{0.5}V_2O_8$ at 75 °C, 125 °C and 250 °C.

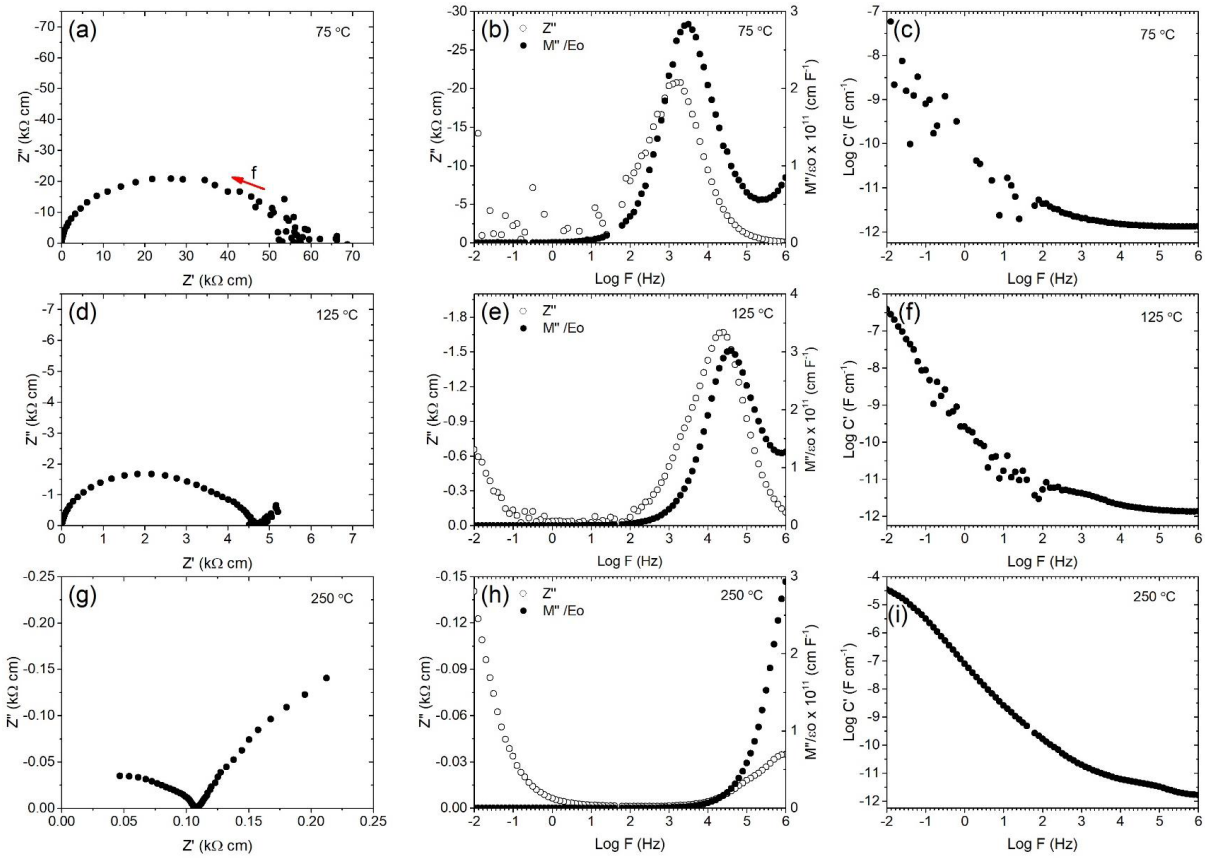

Figure S4 - Impedance complex plane plots (a, d, g) and spectroscopic plots of C'(c, f, i), M" and -Z" (b, e, h) for $Li_{2.75}Ni_{0.5}Cr_{0.75}V_2O_8$ at 75 °C, 125 °C and 250 °C.

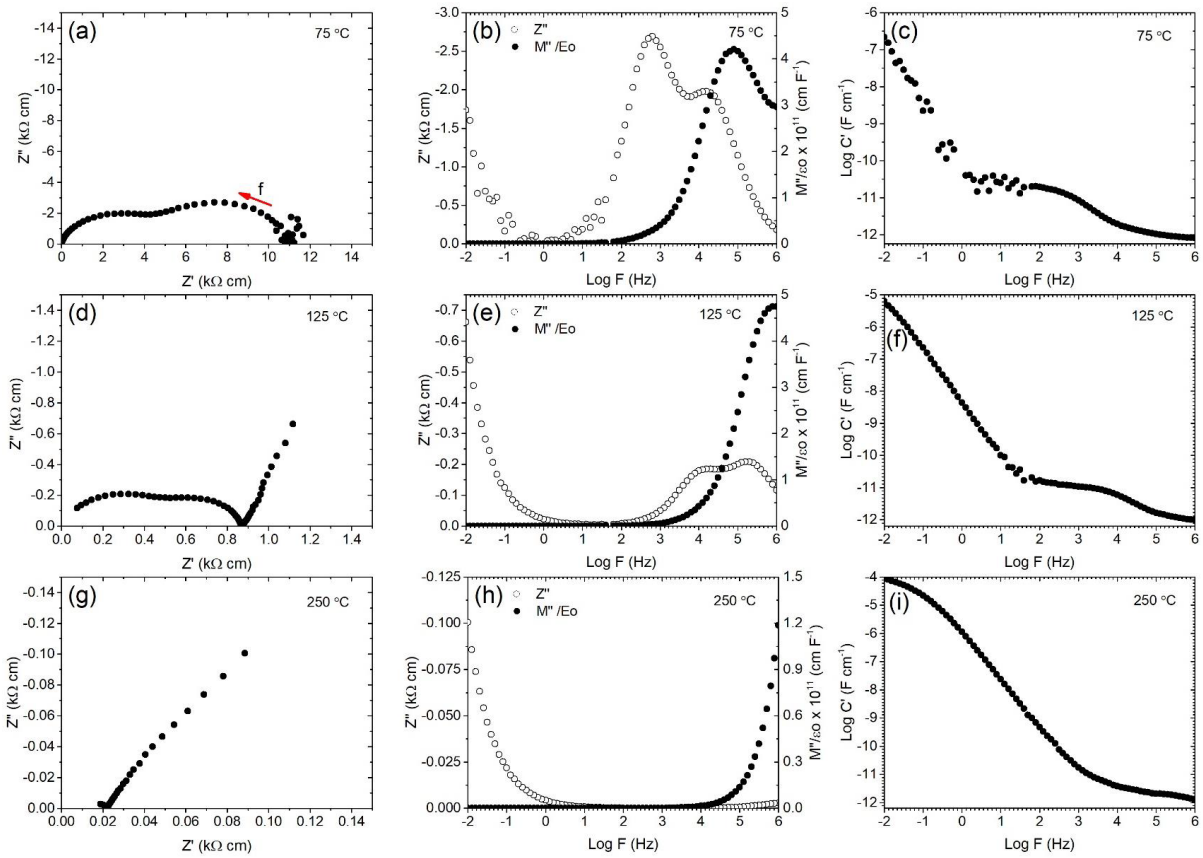

Figure S5 - Impedance complex plane plots (a, d, g) and spectroscopic plots of C'(c, f, i), M" and -Z" (b, e, h) for $Li_3CrV_2O_8$ at 75 °C, 125 °C and 250 °C.

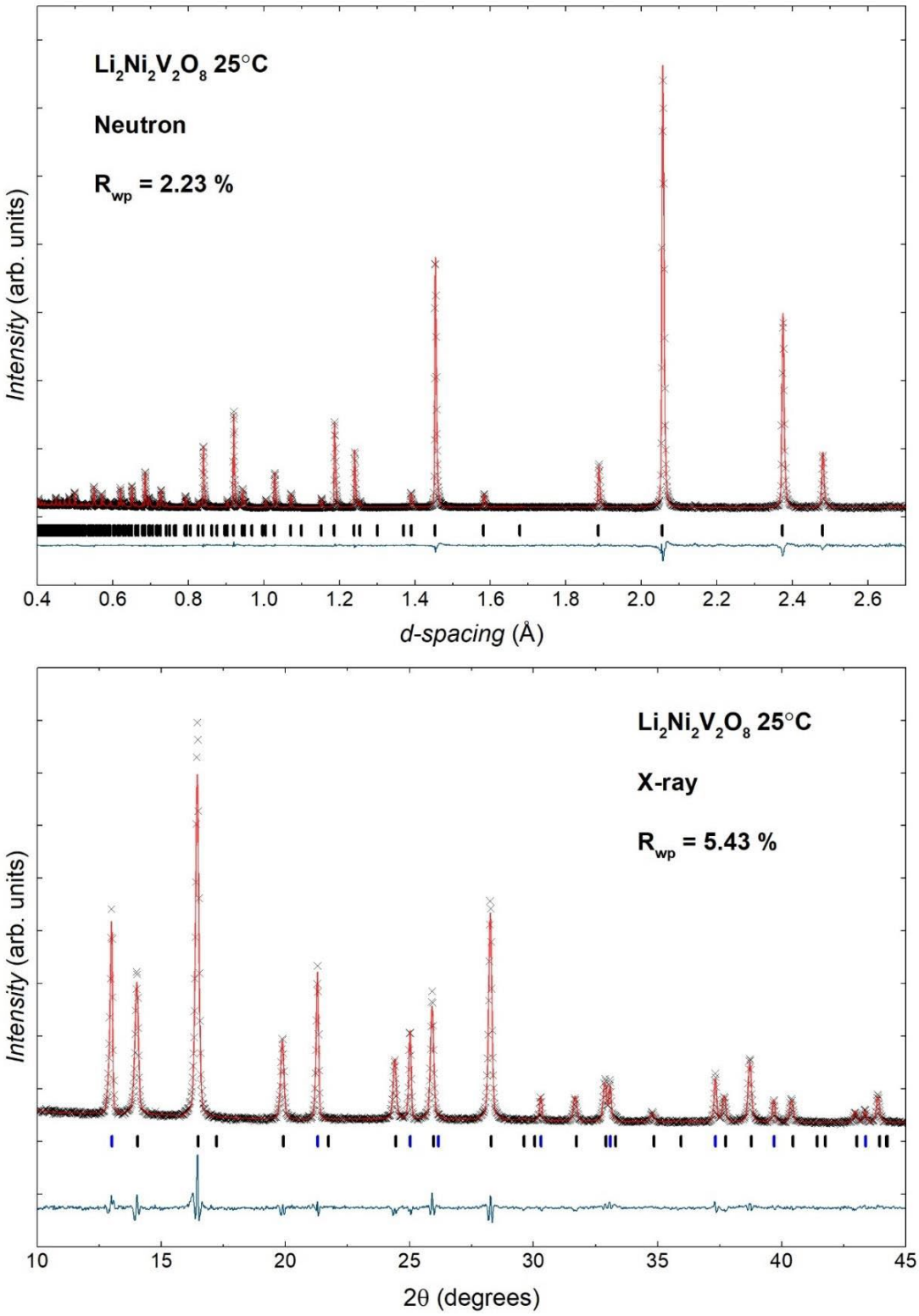

Figure S6. Observed, calculated and difference profiles of combined X-ray and Neutron diffraction data for $Li_2Ni_2V_2O_8$ at 25 °C. Observed data are shown in black crosses, calculated in red, difference in blue and calculated reflection positions as black (spinel phase) and blue (Si standard) tickmarks.

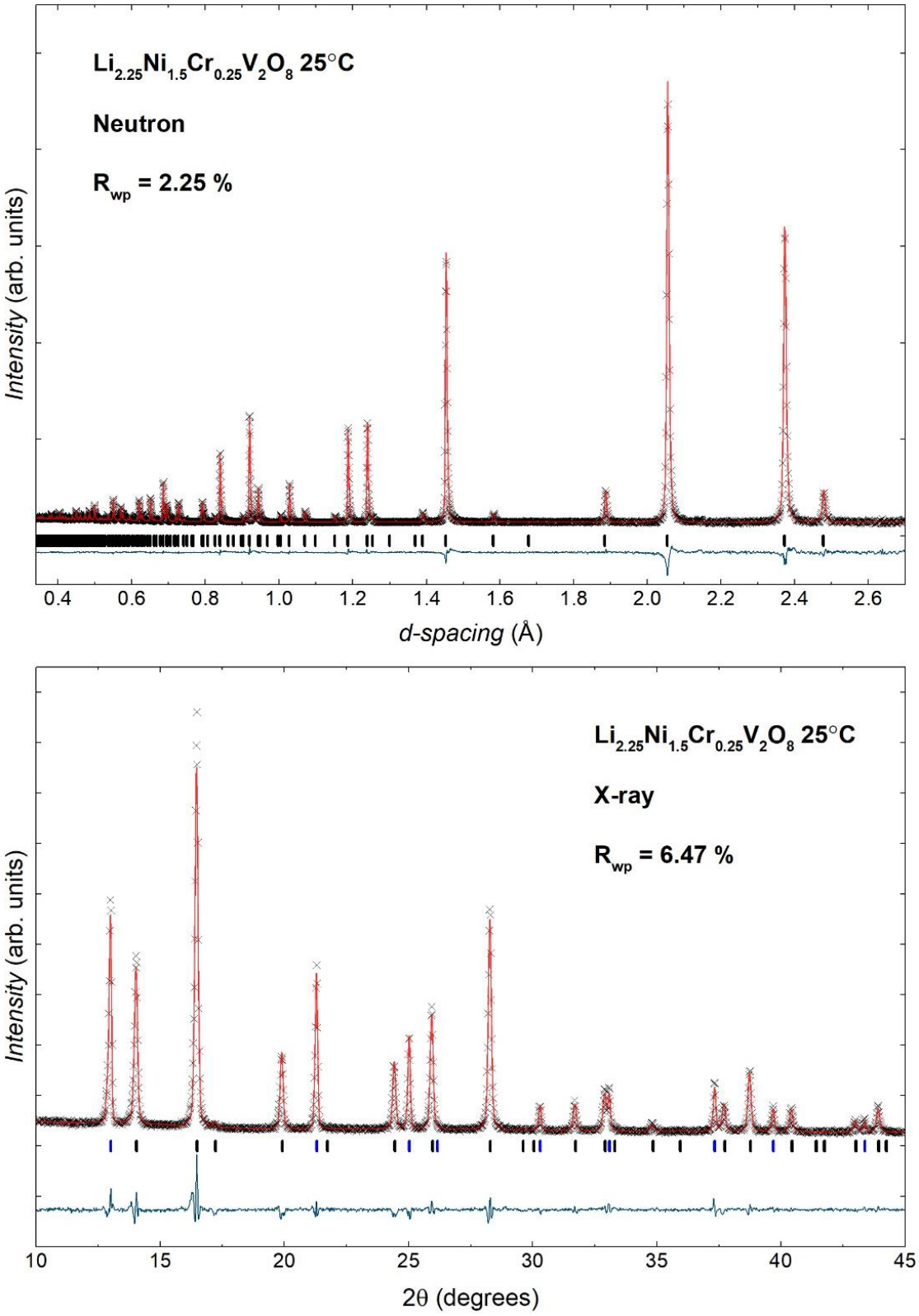

Figure S7. Observed, calculated and difference profiles of combined X-ray and Neutron diffraction data for $Li_{2.25}Ni_{1.5}Cr_{0.25}V_2O_8$ at 25 °C. Observed data are shown in black crosses, calculated in red, difference in blue and calculated reflection positions as black (spinel phase) and blue (Si standard) tickmarks.

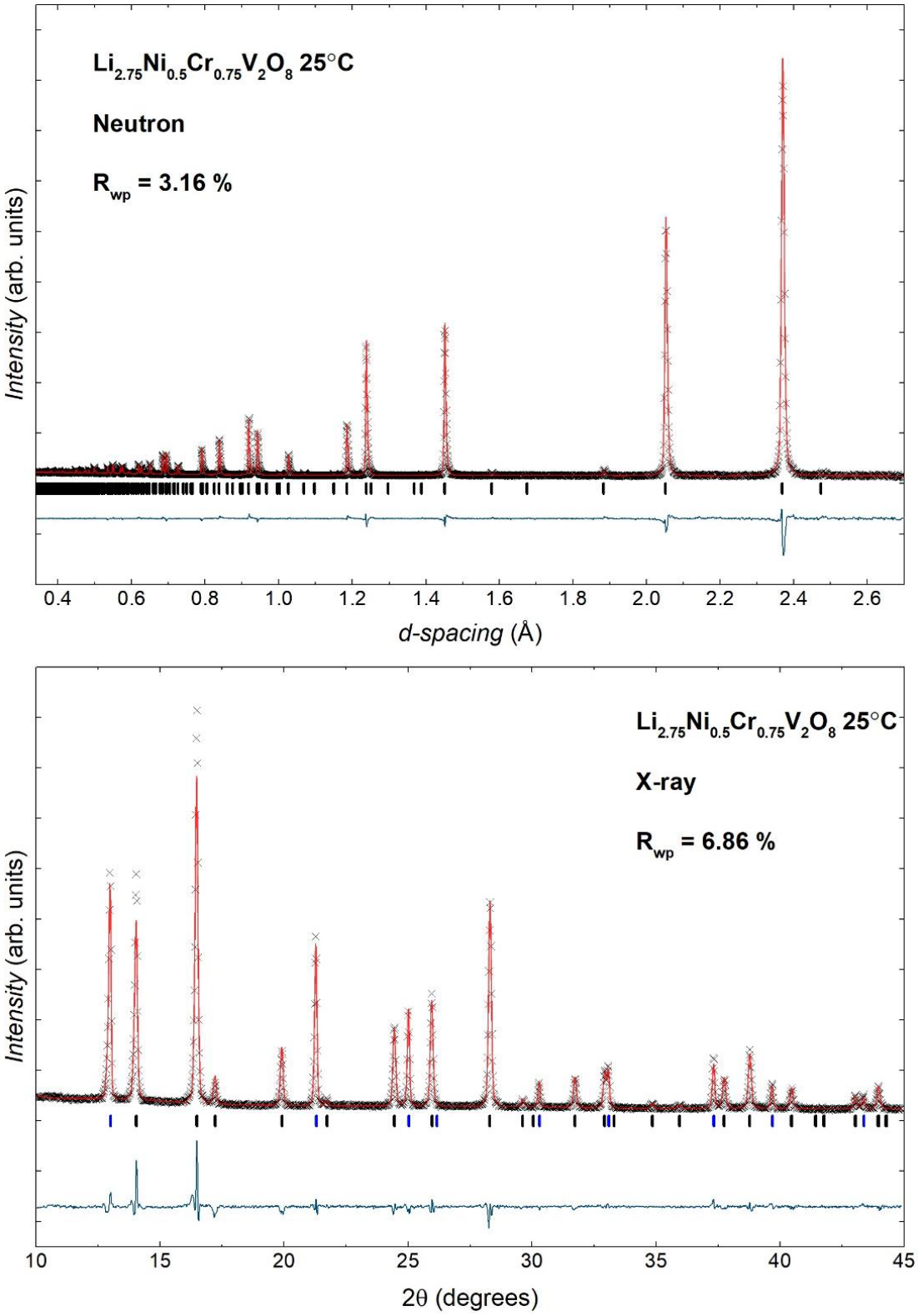

Figure S8. Observed, calculated and difference profiles of combined X-ray and Neutron diffraction data for $Li_{2.75}Ni_{0.5}Cr_{0.75}V_2O_8$ at 25 °C. Observed data are shown in black crosses, calculated in red, difference in blue and calculated reflection positions as black (spinel phase) and blue (Si standard) tickmarks.

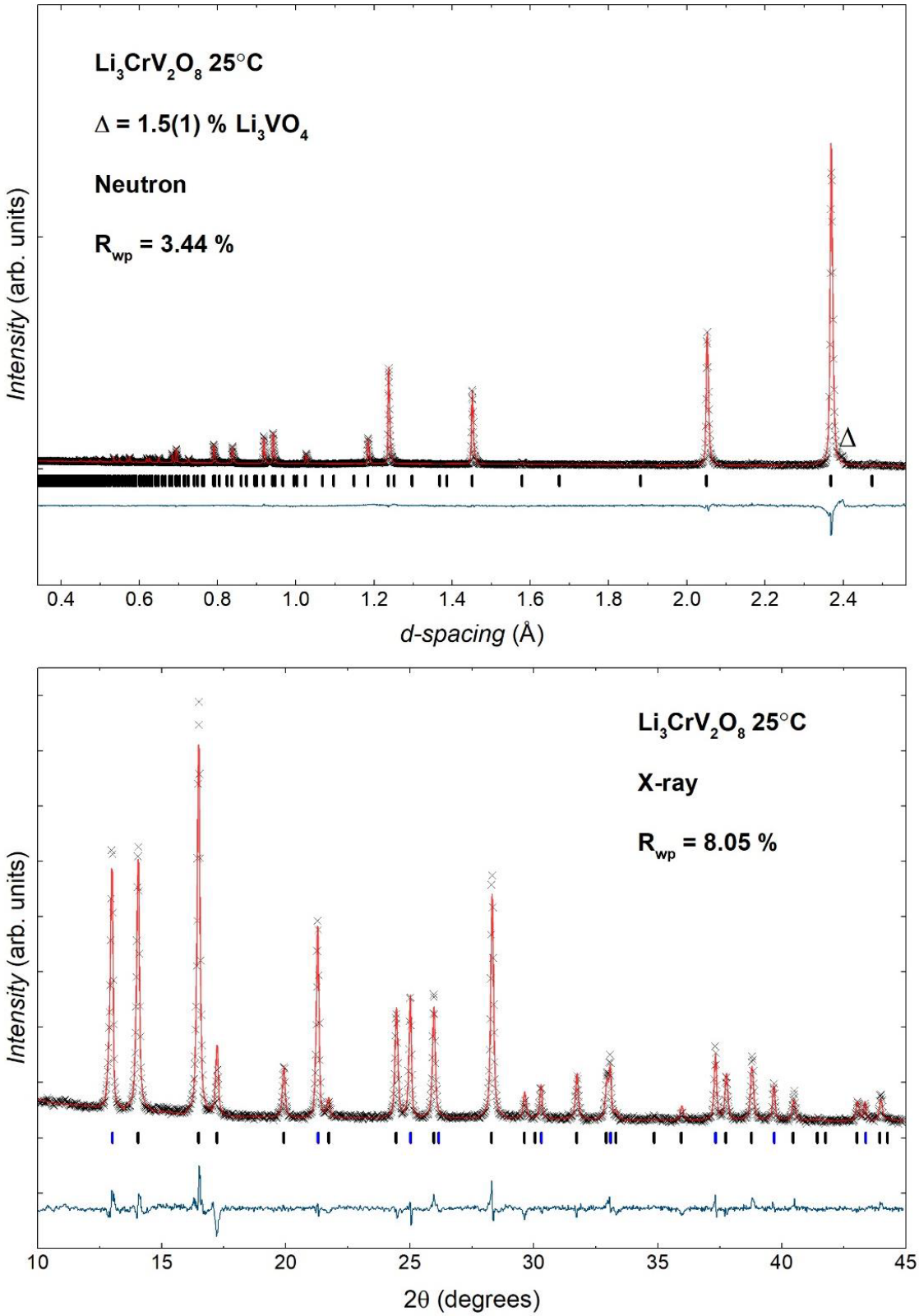

Figure S9. Observed, calculated and difference profiles of combined X-ray and Neutron diffraction data for $Li_3CrV_2O_8$ at 25 °C. Observed data are shown in black crosses, calculated in red, difference in blue and calculated reflection positions as black (spinel phase) and blue (Si standard) tickmarks.

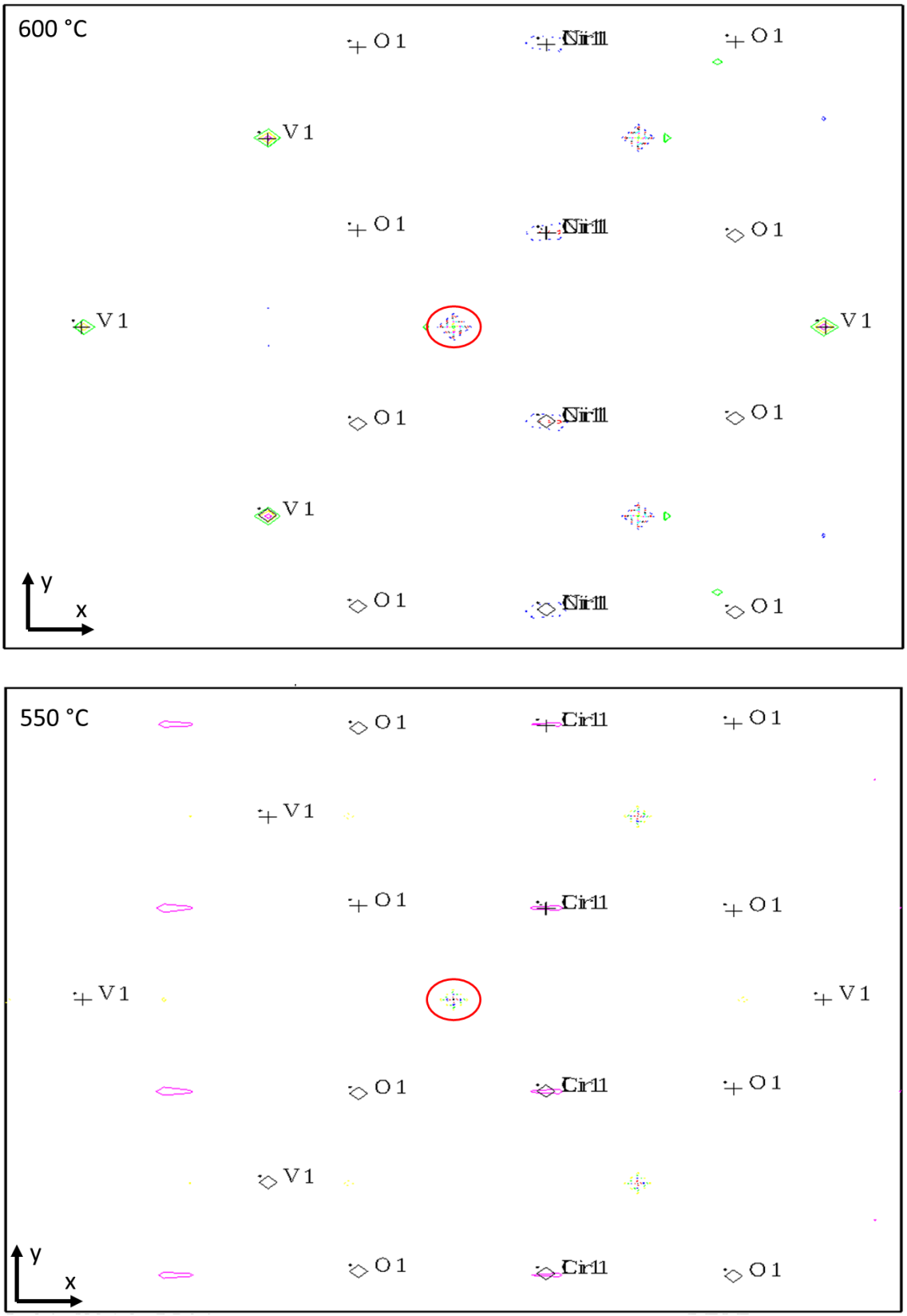

Figure S10. Difference Fourier maps calculated for (a) $Li_{2.5}NiCr_{0.5}V_2O_8$ at 600 °C, and (b) $Li_3CrV_2O_8$ at 550 °C. Centre of reference is 0.125, 0.125, 0.125, with a map size of 10 Å × 10 Å. Solid and dash lines represent contours of positive and negative scattering density, respectively. Significant negative scattering is located between V1 atoms, which can be attributed to Li in 8*a* tetrahedral sites.

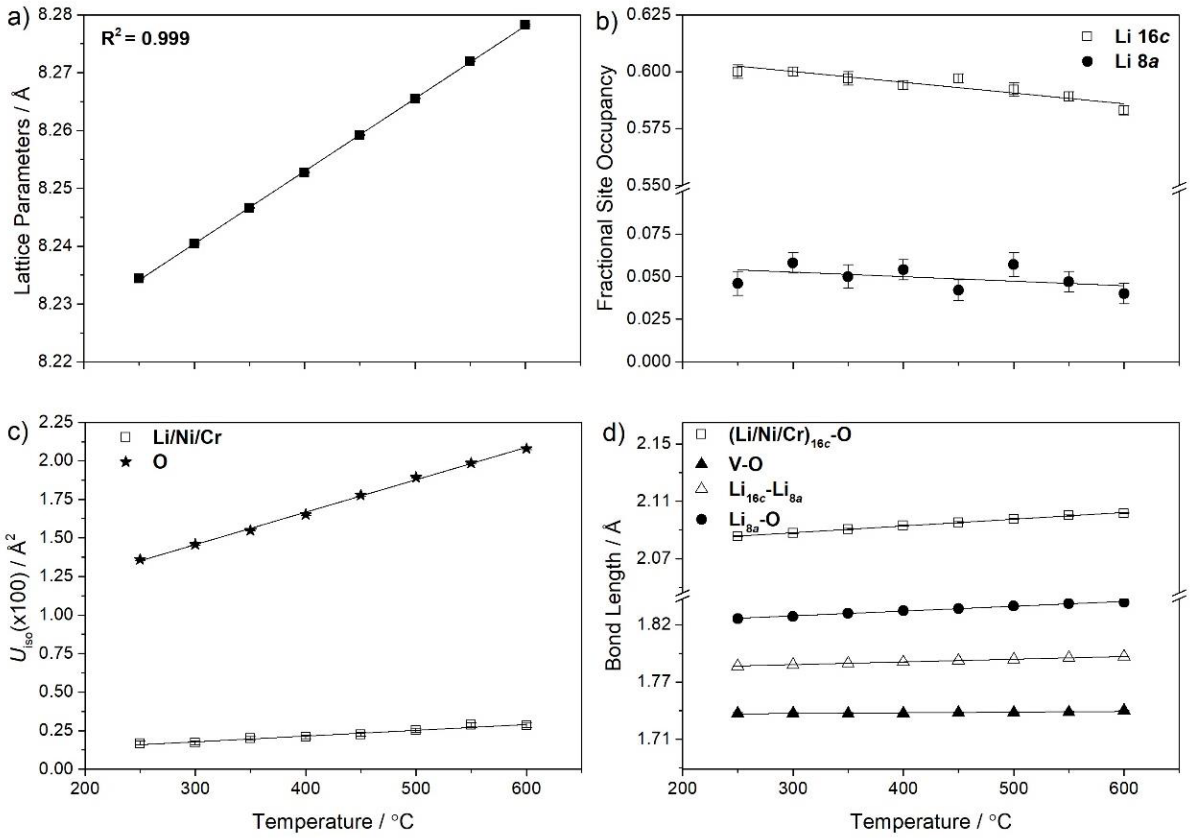

Figure S11. Structural evolution of $Li_{2.5}NiCr_{0.5}V_2O_8$ with temperature, a) lattice parameters, b) fractional site occupancy of Li in 16*c* and 8*a* sites, c) thermal displacement parameters and d) variation of bond lengths. Some estimated standard deviations are smaller than the symbols.

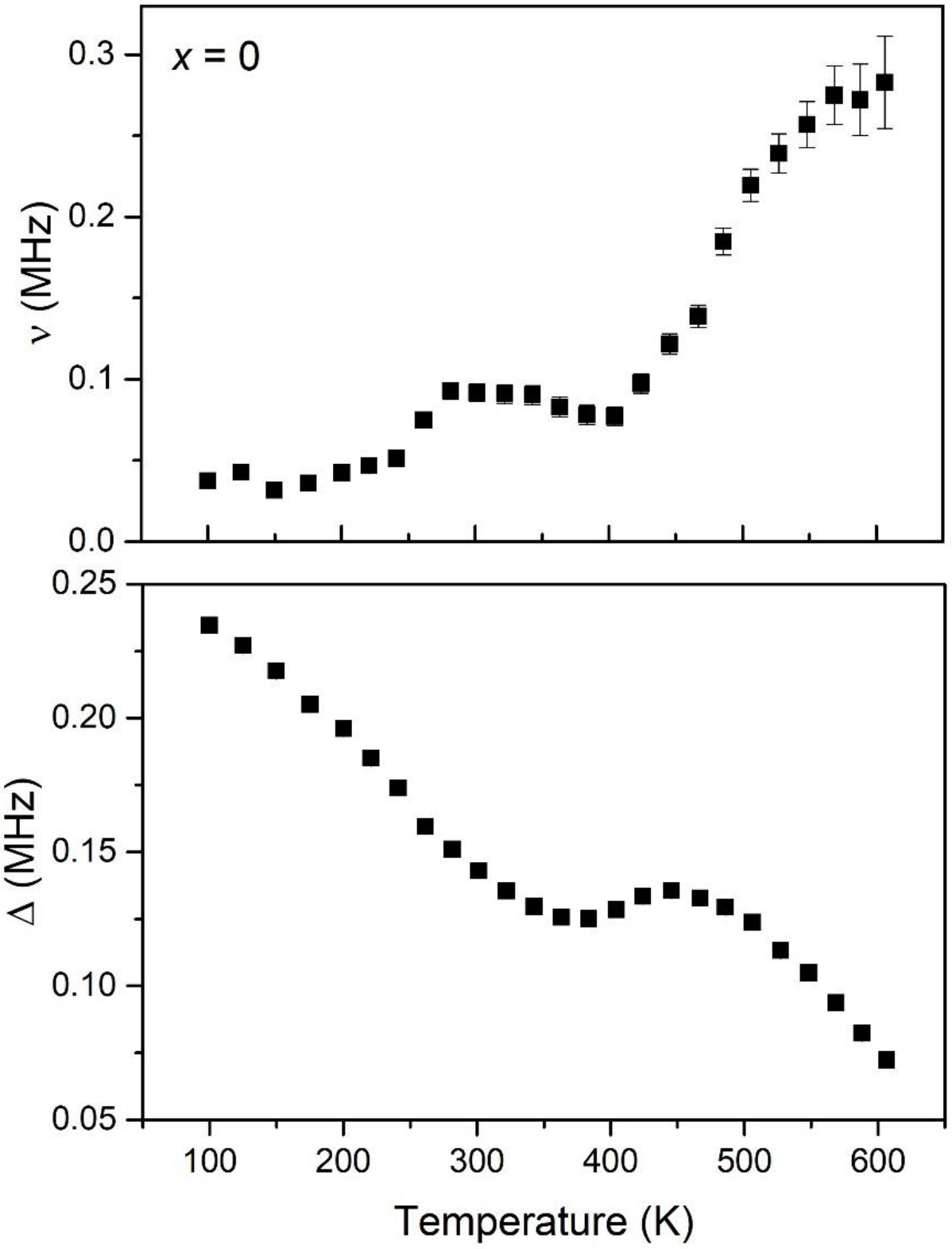

Figure S12. Variation of ν and Δ with temperature obtained from the fitting of raw asymmetry data to Equation 5.1 for $Li_{2+x}Ni_{2-2x}Cr_xV_2O_8$, x = 0, measured from 100 K to 600 K.

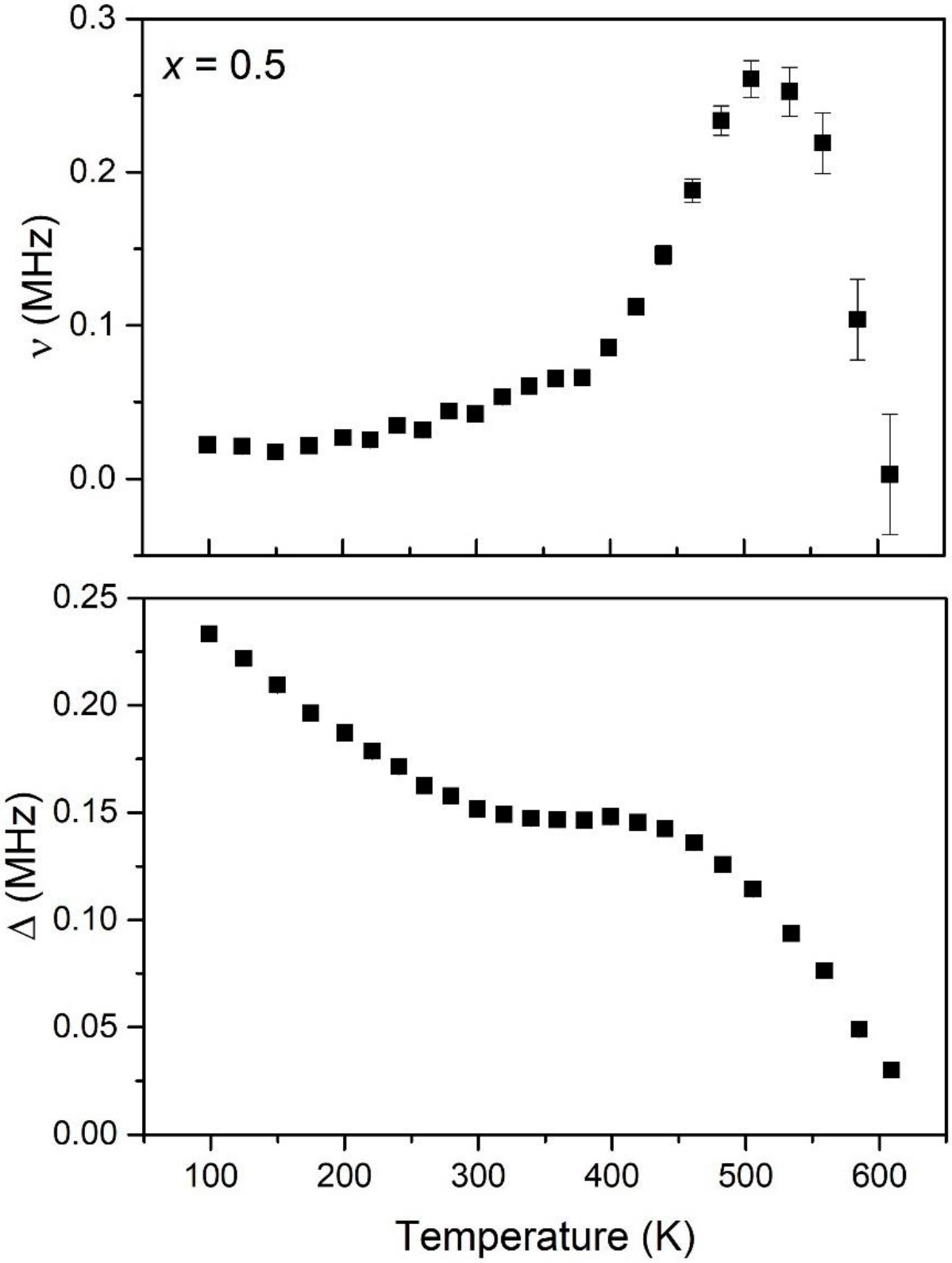

Figure S13. Variation of ν and Δ with temperature obtained from the fitting of raw asymmetry data to Equation 5.1 for $Li_{2+x}Ni_{2-2x}Cr_xV_2O_8$, x = 0.5, measured from 100 K to 600 K.

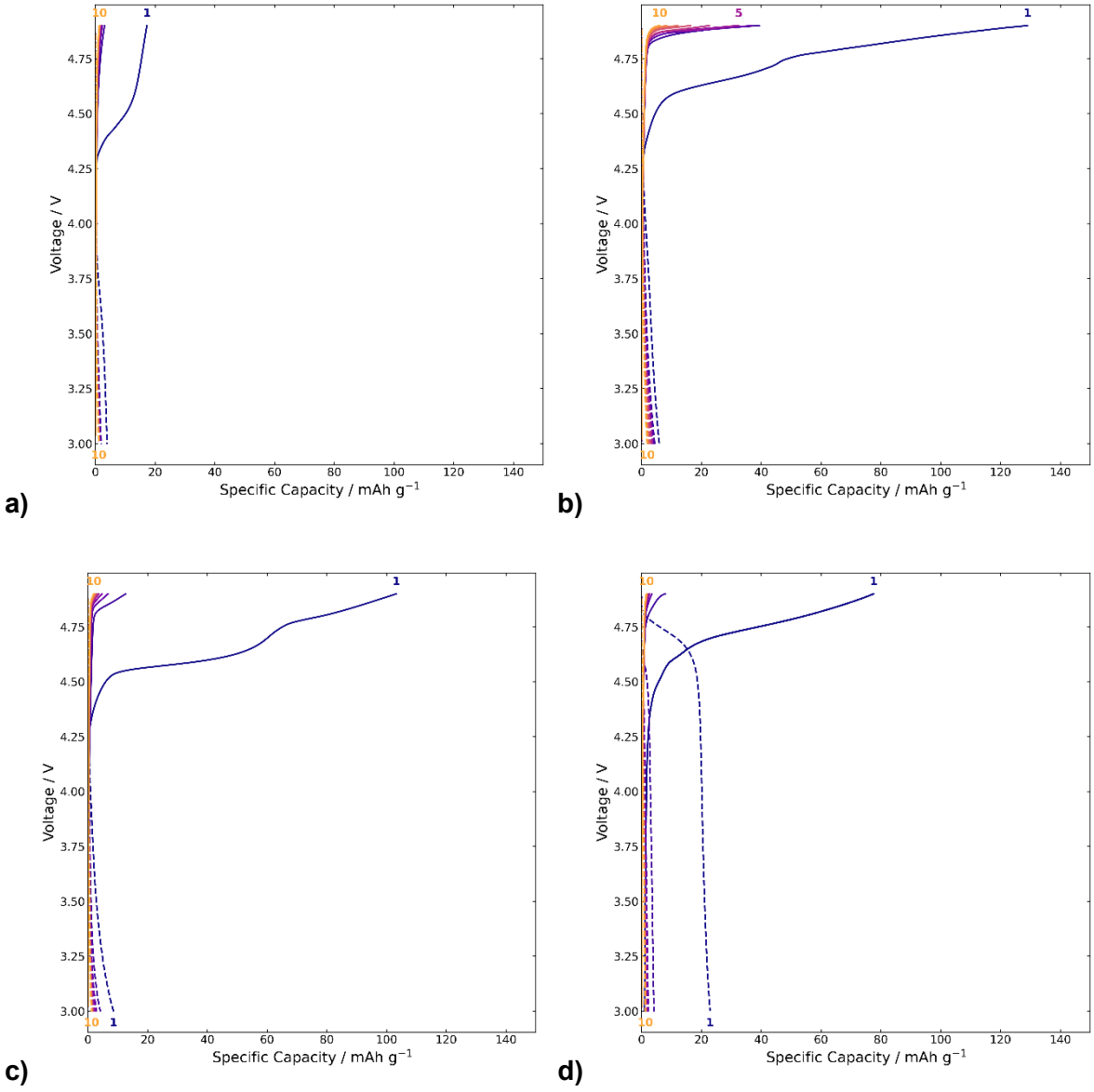

Figure S14. Electrochemical data for $Li_{2+x}Ni_{2-2x}Cr_xV_2O_8$ (a: x = 0, b: x = 0.25, c: x = 0.5, and d: x = 1.0) for the first 10 charge and discharge cycles when cycled between 3 V and 4.9 V at C/10 rate.

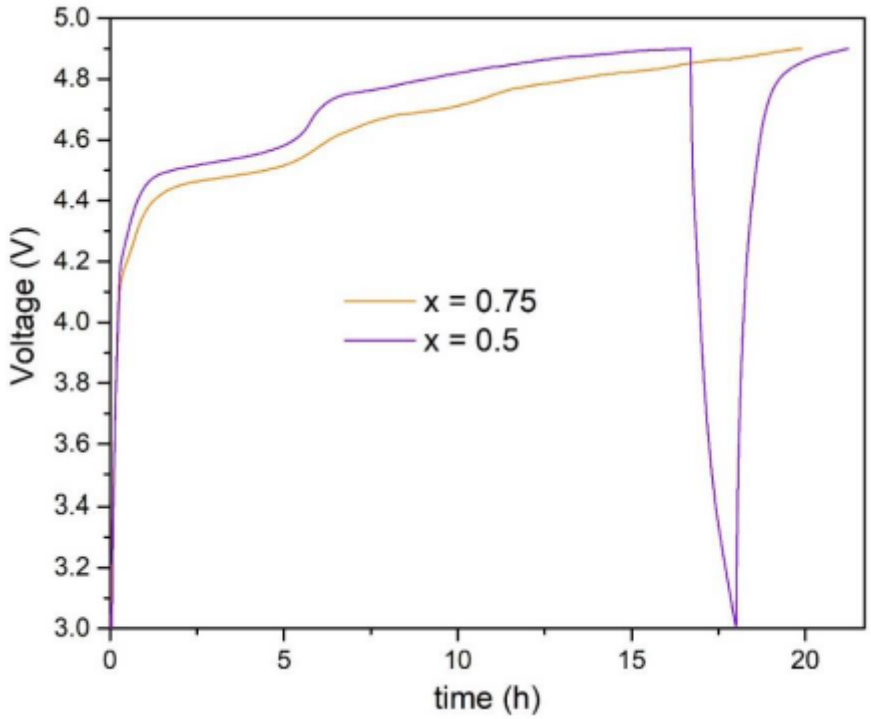

Figure S15. *In situ* electrochemical data for x = 0.75 and x = 0.5, cycled between 3 V to 4.9 V at a C-rate of C/20 and C/15 respectively. A connection issue affected data collection for a short period during cell cycling on the beamline overnight for x = 0.5.

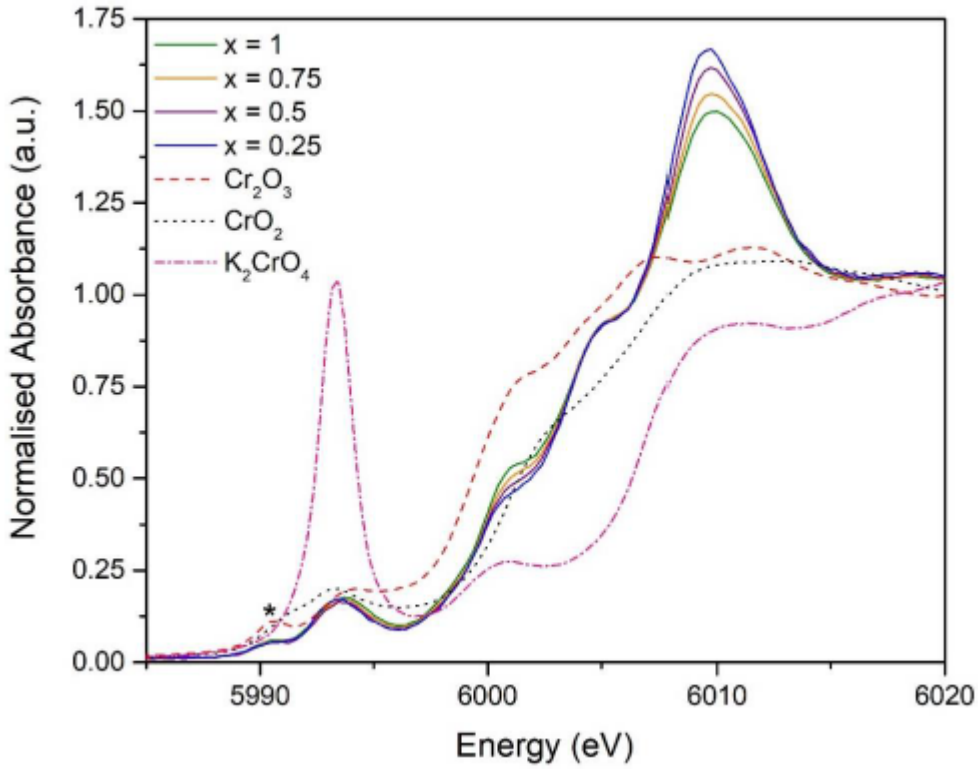

Figure S16. Normalised Cr *K*-edge XANES spectra for powder samples of $Li_{2+x}Ni_{2-2x}Cr_xV_2O_8$ (x = 0.25, 0.5, 0.75, and 1) and the standard reference materials Cr_2O_3 (Cr^{3+}), CrO_2 (Cr^{4+}) and K_2CrO_4 (Cr^{6+}). The first pre-edge feature is marked with an asterisk, *.

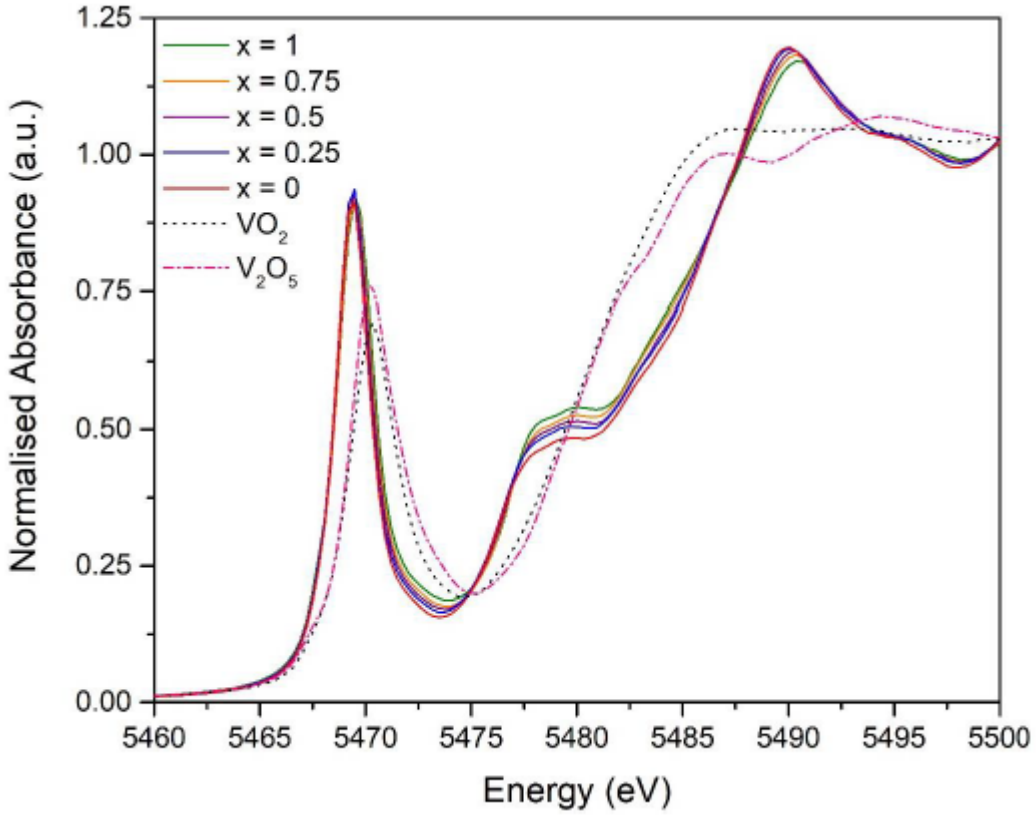

Figure S17. Normalised V *K*-edge XANES spectra for $Li_{2+x}Ni_{2-2x}Cr_xV_2O_8$ (x = 0, 0.25, 0.5, 0.75, and 1) and the standard reference materials, VO_2 and V_2O_5.

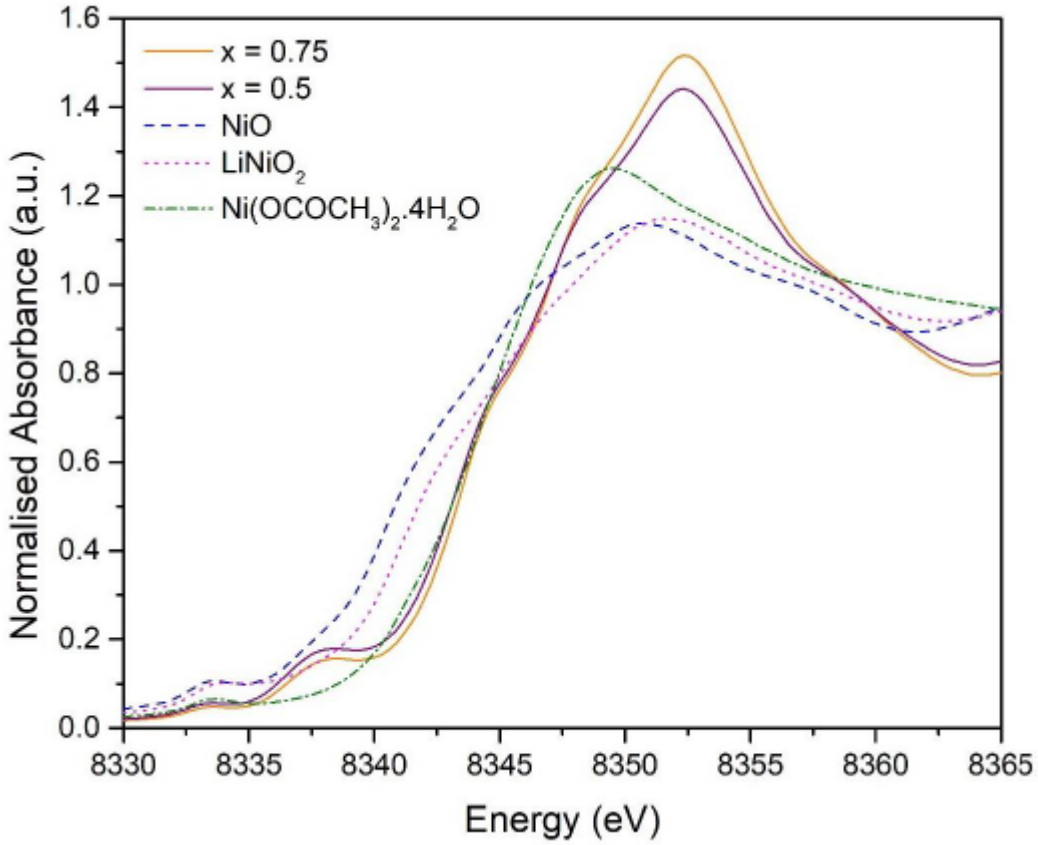

Figure S18. Normalised Ni *K*-edge XANES spectra for $Li_{2+x}Ni_{2-2x}Cr_xV_2O_8$ (x = 0.5 and 0.75) and the standard reference materials, NiO, $LiNiO_2$ and $Ni(OCOCH_3)_2{\cdot}4H_2O$.

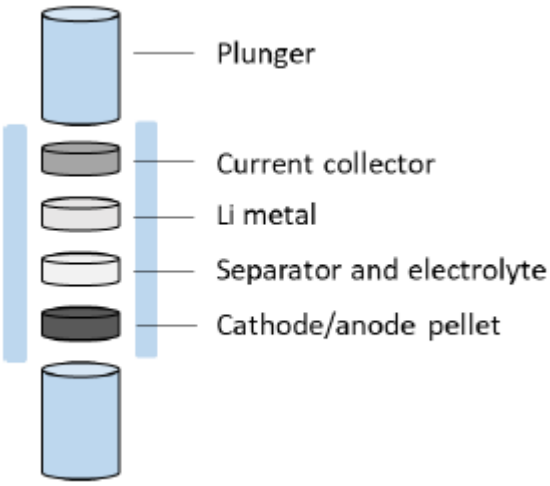

Figure S19. Schematic of the Swagelok cell used for galvanostatic cycling experiments.